Liquid Droplets on a Highly Deformable Membrane

Rafael D. Schulman[1] and Kari Dalnoki-Veress[1,2,*]
[1]Department of Physics and Astronomy, McMaster University, 1280 Main St. W, Hamilton, ON, L8S 4M1, Canada
[2]Laboratoire de Physico-Chimie Théorique, UMR CNRS Gulliver 7083, ESPCI, Paris, France
(Received 12 September 2015; published 9 November 2015)

We examine the deformation produced by microdroplets atop thin elastomeric and glassy free-standing films. Because of the Laplace pressure, the droplets deform the elastic membrane thereby forming a bulge. Thus, two angles define the droplet or membrane geometry: the angles the deformed bulge and the liquid surface make with the film. These angles are measured as a function of the film tension, and are in excellent agreement with a force balance at the contact line. Finally, we find that if the membrane has an anisotropic tension, the droplets are no longer spherical but become elongated along the direction of high tension.

DOI: 10.1103/PhysRevLett.115.206101 PACS numbers: 68.03.Cd, 47.55.D-, 68.08.Bc

The interaction between a liquid's surface tension and a solid's elasticity, or elastocapillarity, is relevant in a wide variety of systems including capillary origami and folding [1–4], soft tissues [5–7], wetting of fibers [8–10], and micropatterning of elastomeric surfaces [11–13]. Despite the multitude of applications utilizing this physics, one of the most fundamental properties has only recently started to be understood: the contact angle of a liquid droplet atop a soft solid [14–17].

On rigid substrates, the contact angle of a droplet can be found through a horizontal force balance between the interfacial tensions of the system, known as Young's law [18]. The vertical component of the force is balanced by the elasticity of the solid. In the opposite regime, a liquid droplet atop a liquid substrate, the contact line geometry is determined by a Neumann construction, in which the interfacial tensions are simultaneously balanced in the vertical and horizontal directions [19,20]. Intermediate to these extremes is a droplet atop a soft surface. In such a case, the liquid contact line deforms the solid into a cusp on a length scale given by the elastocapillary length γ/E, where γ is the surface tension and E is Young's modulus [15–17,21–24]. Microscopically, the contact line geometry and local contact angles are described by Neumann's law balancing the surface tension of the liquid with the surface stresses of the solid-vapor and solid-liquid interfaces. The global contact angle, the angle at which the spherical cap intersects the flat undeformed substrate, satisfies Young's law for droplets larger than γ/E [14–17]. However, droplets on the order of γ/E display global contact angles which deviate from Young's law [15]. Elastocapillary phenomena are also present in rigid materials, such as glasses; however, in such cases γ/E is on the order of the molecular size. Therefore, elastocapillary experiments have been limited to soft materials, with moduli on the order of kilo Pascals, to attain deformations and elastocapillary lengths in the μm range.

Alternatively, the length scale of the deformation can be amplified by selecting a more compliant geometry, such as flexible sheets, fibers, or free-standing films, while employing materials with moduli in the MPa to GPa range [1,3,8–10,25–27]. In a seminal study, the surface tension of droplets on free-standing elastomeric films tens of μm thick generated deformations visible to the naked eye [26]. By modeling the system at the contact line, the authors were able to determine the tensions in their films. However, the tensions were never quantitatively verified using other techniques, and the relevant contact angles of the system were solely used to determine the tension and not compared to theoretical expectations.

In this Letter, we present measurements of the global contact angle of droplets atop thin free-standing films of an elastomer ($E \sim$ MPa) and a glass ($E \sim$ GPa) as a function of the tension within the films. We find the contact angles to be in excellent agreement with a Neumann construction in which interfacial and mechanical tensions are balanced at the contact line. In the limit of high tensions, our model and measured contact angles tend towards Young's law. Finally, we show that droplets placed atop films with an anisotropic biaxial tension become elongated in the direction of high tension.

Elastomeric films with thickness ranging from $h \sim 280$ to 3500 nm were prepared from a styrene-isoprene-styrene (SIS) triblock copolymer and subsequently supported on a washer with a circular hole to produce free-standing films 3 mm in diameter [28]. Free-standing glassy films of poly (n-butyl methacrylate) (PnBMA) with $h \sim 65$ to 140 nm were similarly prepared. For the liquid droplets, we use glycerol and polyethylene glycol (PEG). Droplets were placed on either side of the free-standing film as seen in Fig. 1(a) and viewed from the side with an optical microscope. In this geometry, droplets and bulges could be directly imaged on the top side of the washer (the edges of the washer obscures the bottom side). Images of the corresponding droplets or bulges were also obtained from a top view for a more precise measurement of the contact radii r_c [Fig. 1(a)]. Contact angle measurements were performed within ~4 min of droplet deposition to ensure negligible evaporation of the liquid. We found that the

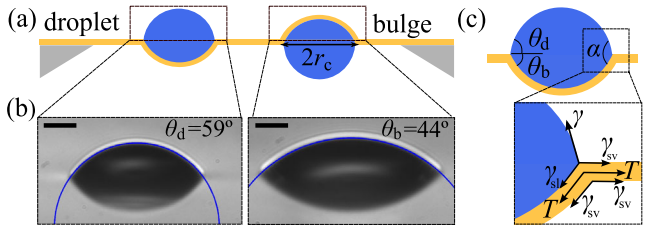

FIG. 1 (color online). (a) Schematic of the side view of liquid droplets on the top and bottom side of the film, not to scale. (b) Microscope images of the side view of a droplet (left) and bulge (right). The top half of the image is the direct visualization of the droplet or bulge, while the bottom half corresponds to a reflection off the film itself. The curves represent spherical cap fits to the profiles. The scale bar represents 20 μm. (c) Schematic of a droplet and bulge with the relevant angles identified. The expanded view shows the interfacial and mechanical tensions acting on the contact line.

contact radii and contact angles of sufficiently large droplets ($r_c > 25$ μm) exhibited negligible change over this experimental time scale. Therefore, our measurements were limited to droplets with $r_c > 25$ μm to be completely confident that evaporation does not play a role.

Examples of optical images of a droplet and bulge are shown in Fig. 1(b). The droplet or bulge profiles are well fit to spherical caps, represented by curves in Fig. 1(b). From each fit, we extract the radius of curvature, R_d or R_b, for droplets and bulges. The droplet and bulge contact angles [Fig. 1(c)], θ_d and θ_b, are defined as the contact angles with which the respective spherical caps intersect the undeformed film and are calculated using the identities $\sin\theta_d = r_c/R_d$, $\sin\theta_b = r_c/R_b$. We find that the contact angles show no systematic dependence on droplet size within the range investigated ($r_c \sim 25$–200 μm). Therefore, on a given sample, several droplets and bulges are deposited and average values of θ_d and θ_b are found. The total internal liquid angle α is simply the sum of the average values of θ_d and θ_b.

As will be justified below, we make the reasonable assumption that only tensile forces (surface tensions and mechanical tension in the film) are relevant and that bending can be neglected. The elastocapillary length (<100 nm) in our system is much smaller than the size of our droplets, so surface stresses of the solid or ridges at the contact line do not influence the global contact angles we measure. Furthermore, the droplet sizes employed are well below the capillary length of the system. Thus, gravitational effects are negligible. In this limit, the film deformation can be understood rather simply. The Laplace pressure within the droplet causes the film below it to bulge into a spherical cap. Outside the droplet, the film is undeformed and flat. In addition, as seen in Fig. 1(c), the contact line geometry results from a force balance between the interfacial tensions of the system and the mechanical tension T within the film. Analogous to a Neumann construction, the liquid-vapor γ, solid-liquid γ_{sl}, and solid-vapor surface tensions γ_{sv} tug at the triple point. However, we must also include the additional contributions from the mechanical tension in the film, as well as the solid-vapor surface tensions present on the opposite side of the film. We label the three tensions pulling the film down as $T_{in} \equiv T + \gamma_{sl} + \gamma_{sv}$ and the three tensions pulling away from the droplet as $T_{out} \equiv T + 2\gamma_{sv}$. We assume that T is the same in the region under the droplet compared to outside the droplet. From the definitions of T_{in} and T_{out}, we see that $T_{out} = T_{in} - \gamma_{sl} + \gamma_{sv} = T_{in} + \gamma\cos\theta_y$, where θ_y is the Young's angle of the liquid atop a supported substrate of the material, which we measure independently. A vertical force balance at the contact line yields

$$\frac{T_{in}}{\gamma} = \frac{\sin\theta_d}{\sin\theta_b}, \tag{1}$$

which can also be attained by balancing the Laplace pressure with the restorative pressure from the film. Equation (1) is convenient: the normalized tension T_{in}/γ is obtained from the measured angles θ_d and θ_b. A similar approach (assuming $\alpha = \theta_y$) has been employed to determine tensions in thicker films [26]. Furthermore, we use the cosine law to obtain

$$\cos\theta_d = \frac{(T_{out}/\gamma)^2 + 1 - (T_{in}/\gamma)^2}{2T_{out}/\gamma} \tag{2a}$$

$$\cos\theta_b = \frac{(T_{out}/\gamma)^2 - 1 + (T_{in}/\gamma)^2}{2T_{out}T_{in}/\gamma^2}, \tag{2b}$$

where we have made use of the fact that the film is flat outside the droplet. Since $T_{out} = T_{in} + \gamma\cos\theta_y$, we see that Eq. (2) allows us to predict the individual contact angles knowing the Young's angle and the normalized tension T_{in}/γ given by Eq. (1). Similarly, the total internal angle α is given by

$$\cos\alpha = \cos\theta_y - \frac{\gamma}{2T_{in}}\sin^2\theta_y. \tag{3}$$

In the limit of $T_{in}/\gamma \to \infty$ the equations reduce to $\theta_d \to \theta_y$, $\alpha \to \theta_y$, and $\theta_b \to 0$. That is, in the limit of high tensions, we recover Young's law, since the droplet is sessile on a completely rigid substrate. In Figs. 2(a) and Fig. 2(b) we plot our data for θ_d and θ_b as a function of T_{in}/γ found using Eq. (1) for glycerol on SIS and PnBMA. The droplet contact angle increases with increasing tension while the bulge contact angle decreases as the surface becomes less deformable at high tensions. Various tensions were achieved by changing film thickness and through sample-to-sample variation [29]. We find thicker films to have a higher tension, in accordance with previous work [26]. In Fig. 2(c) we plot the total internal liquid angle α

against the normalized tension and find it to decrease with higher tension. It is important to note that at all finite tensions one has $\theta_d < \theta_y$ while $\alpha > \theta_y$. This result is in contrast with previous studies which have assumed α to be constant and equal to the contact angle on a supported substrate [26,27]. In Figs. 2(a)–2(c), the predictions of Eqs. (2) and (3) are plotted, with the Young's angle of glycerol atop SIS fixed to $81 \pm 1.5°$. The simple force balance at the contact line captures the data, validating that at finite tensions the contact angles can be found through a Neumann construction which includes interfacial and mechanical tensions. As $T_{in}/\gamma \to \infty$ Young's law is recovered. In Figs. 2(a)–2(c) the SIS and PnBMA data are found to collapse onto the same curve, despite being completely different materials. This collapse is due to the coincidental fact that Young's angle of glycerol on SIS is equal to the Young's angle of glycerol on PnBMA ($82.5 \pm 1.5°$) within experimental error. Since the theoretical curves are completely determined by T_{in}/γ (as seen in the plots) and θ_y, the data fall along the same curve.

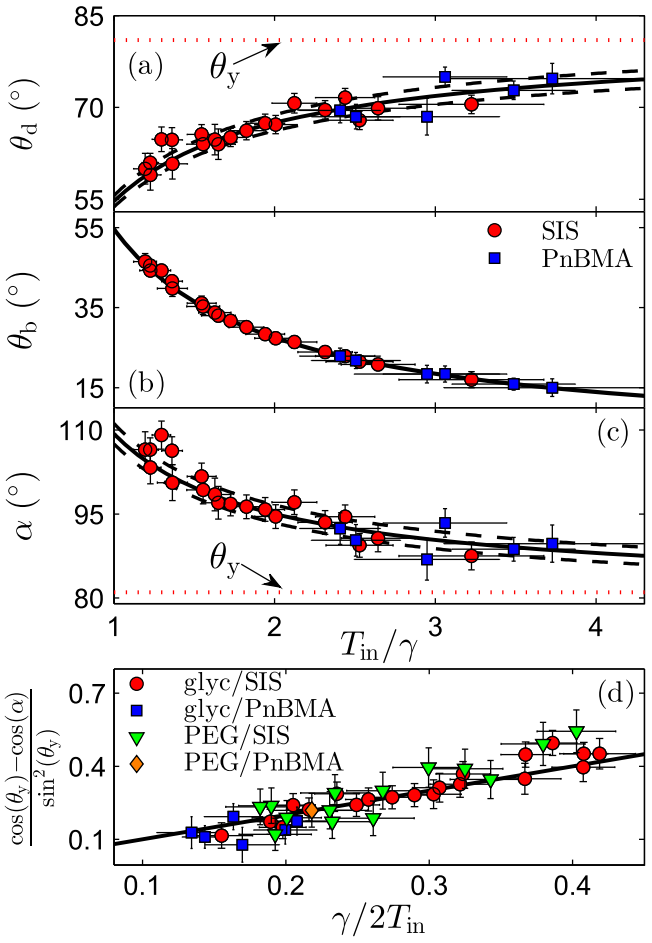

FIG. 2 (color online). (a) The droplet contact angle, (b) the bulge contact angle, and (c) the total internal liquid angle plotted as a function of the normalized tension [see Eq. (1)] for glycerol on SIS (circles) and glycerol on PnBMA (squares). The curves are Eq. (2) and Eq. (3) with θ_y given by the Young's angle of glycerol on SIS (represented by the dotted horizontal lines). The dashed black lines are bounds to the theory due to uncertainty in θ_y. The uncertainty in the theoretical curve for θ_b is on the order of the thickness of the curve itself. (d) $(\cos\theta_y - \cos\alpha)/\sin^2\theta_y$ as a function of $\gamma/2T_{in}$ for four liquid-substrate combinations. The black line is the theoretical prediction. The vertical and horizontal error bars stem from uncertainties in the measured values of θ_d and θ_b.

In the model, we assume the mechanical tension T to be the same in the region under the droplet compared with the rest of the film. In fact, the theoretical curves in Figs. 2(a)–2(c) are remarkably sensitive to this assumption. If we, for instance, enforce the two tensions to differ by as little as 5 mN/m (which corresponds to only 7% of T_{in} for the lowest tension data), the theoretical curves are inconsistent with the data [28]. Therefore, the assumption of constant mechanical tension throughout the film must be valid.

We also perform experiments with another liquid, PEG, atop SIS and PnBMA, for which the Young's angle is substantially different from glycerol ($55.3 \pm 1.5°$ and $58.4 \pm 1.5°$). To demonstrate that the theory is valid for all tested combinations of liquid and substrate material, we can rearrange Eq. (3) into the following form $(\cos\theta_y - \cos\alpha)/\sin^2\theta_y = \gamma/2T_{in}$. In Fig. 2(d), we plot the left hand side of this equation against $\gamma/2T_{in}$ for the four liquid-substrate combinations tested. As expected, these data all fall along a line of unity slope passing through the origin. The measured droplet and bulge contact angles are also well predicted by Eq. (2) for PEG [28].

In our experiments, we obtain T_{in}/γ from $\sin\theta_d/\sin\theta_b$. Although this procedure was used in a previous study, the tensions were never quantitatively verified using alternate methods [26]. In order to completely demonstrate the success of the model, we must test the measured tensions against some predictions. First, if the tension of the same film is measured with two different liquids, glycerol, and PEG, then $T_{in,PEG} = T_{in,glyc} - \gamma_{sl,PEG} + \gamma_{sl,glyc} = T_{in,glyc} - \gamma_{glyc}\cos\theta_{y,glyc} + \gamma_{PEG}\cos\theta_{y,PEG}$, where subscripts PEG and glyc denote the two liquids. Substituting in literature values for $\gamma_{PEG} = 46$ mN/m and $\gamma_{glyc} = 63$ mN/m [30,31], the expected relationship becomes $T_{in,PEG} = T_{in,glyc} - (16 \pm 3$ mN/m). We performed simultaneous tension measurements using the two liquids atop SIS as seen in Fig. 3(a). The data are well fit to a line of slope 0.98 ± 0.07 and intercept of -22 ± 8 mN/m, which agrees with the theoretical result within error. The difference in the intercept can be explained by discrepancies in the literature values of γ for our liquids.

To further validate the tensions obtained with the droplets, we also measure the tensions mechanically using a home built micropipette deflection apparatus [32]. In this technique, the tip of a flexible micropipette, which serves as a force transducer, is pressed against the film. In doing so, the deformation of the membrane as well as the force acting

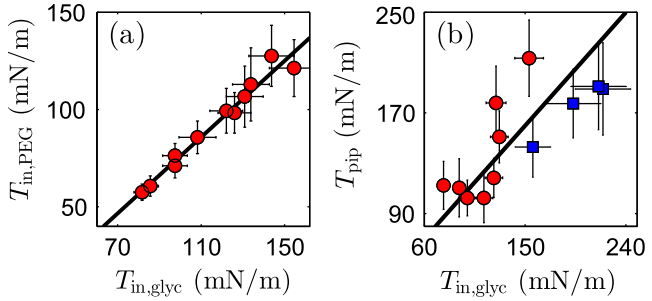

FIG. 3 (color online). (a) The tension as measured with PEG compared to those measured with glycerol on the *same* SIS sample. The black line is a linear fit to the data. (b) The tension as measured with micropipette deflection correlated to those measured with glycerol on SIS (circles) and PnBMA (squares). The black line represents the theoretical relationship, where the thickness of the line is indicative of its upper and lower bound given uncertainties in θ_y. Error bars for liquid tensions stem from uncertainties in determining θ_d and θ_b, whereas error bars for pipette tensions arise from uncertainties in the spring constant of the pipette as well as in measuring the deformation of the film.

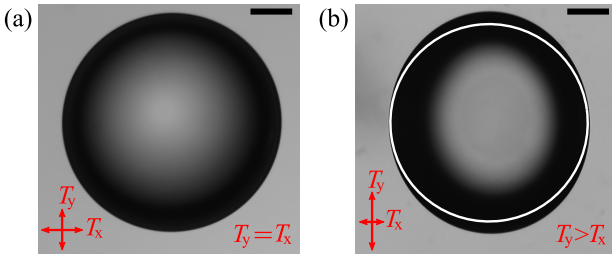

FIG. 4 (color online). (a) Top view of a water droplet atop a SIS film with isotropic tension ($T_x = T_y$). The droplet is round when viewed from above. (b) Top view of a water droplet atop a SIS film which has been stretched in the y direction ($T_y > T_x$). A white circle is superimposed to emphasize that the droplet is elongated along the direction of high tension. The scale bar represents 50 μm.

on it are known. Since the shape of a taut membrane between two axisymmetric rings (the pipette tip and washer) is known [33], we can determine the tension from the force-deformation data. The measured tension must be equal to $T_{\mathrm{pip}} = T + 2\gamma_{\mathrm{sv}} = T_{\mathrm{in}} + \gamma\cos\theta_y$. Measurements were carried out on both SIS and PnBMA films [34], and the results of T_{pip} as a function of $T_{\mathrm{in,glyc}}$ are displayed in Fig. 3(b). The data are in agreement with the expected trend. Any systematic differences between the SIS and PnBMA data can be attributed to differences in adhesion between the pipette and the respective films, as well as bending being locally important near the pipette tip and influencing the measured tensions. The pipette measurements are prone to scatter due to the alignment of the pipette relative to the film. As evidenced by the significantly reduced scatter in Fig. 3(a), we conclude that tension is more accurately measured using the droplet technique. These tests show that the model is fully consistent in terms of both tension and contact angle data.

Recently, there has been disparity in the literature regarding whether or not the surface tension of an elastomeric film is equal to its surface free energy [26,35]. Following the procedure of Ref. [26], the surface tension of the film can be found by computing the extrapolated zero-thickness value of T_{in} for a SIS film with glycerol droplets. In doing so, we find that $T_{\mathrm{in}} \sim 60$ mN/m. This surface tension compares well with the surface free energy of the film under the droplet, given by $\gamma_{\mathrm{sv}} + \gamma_{\mathrm{sl}} = 2\gamma_{\mathrm{sv}} - \gamma\cos\theta_y \sim 50$ mN/m [36–38].

In this Letter, we make the assumption that our system is dominated by tension and that bending can be neglected. That is, stretching dominates, and the influence of bending is only manifested in a small region around the contact line of characteristic size $\sqrt{Eh^3/12T_{\mathrm{tot}}}$, where T_{tot} is the total tension in the film [26,27]. In our experiments this region is maximally ~ 4 μm but most typically below ~ 2 μm, and thus small in comparison to the droplet sizes employed in this study, indicating that bending can be safely ignored in both materials. The fact that bulges and droplets are well fit to spherical caps and that the contact angles are size independent further validates the assumption.

We have performed experiments with droplets atop thin free-standing films, wherein the surface tension of the liquid produces significant deformation of the film. We measure contact angles of the droplets and bulges relative to the flat film, as well as the total internal liquid angle, and find these to be well described by a Neumann construction in which the interfacial and mechanical tensions are balanced at the contact line. In the high tension limit, the film is essentially undeformable, and Young's law is recovered. Conversely, in the limit of vanishing mechanical tension, we expect to recover the classical Neumann construction where only interfacial tensions are balanced. The tensions we measured using the droplet experiments, which have contributions from both mechanical and interfacial tensions, were quantitatively verified using a purely mechanical technique and by comparing the measured tensions from two different liquids. The experiments described in this manuscript were carried out on a film with a constant isotropic tension, in which case the droplets are perfectly round when viewed from above, as seen in Fig. 4(a). However, an interesting option exists that does not for a droplet on a simple liquid: if a film is floated onto a support and then preferentially stretched along one axis, then the droplets no longer assume a circular equilibrium contact. In Fig. 4(b), a liquid droplet has been placed atop a film which has been stretched in the vertical (y) direction. The droplets become elongated along the axis of higher tension which provides an exciting opportunity for studying equilibrium liquid droplets that deviate from the expected geometry.

The authors are grateful to Anand Jagota, René Ledesma-Alonso, Elie Raphaël, and Thomas Salez for

valuable discussions. Discussions with Salez and Raphaël stimulated these experiments. The financial support by Natural Science and Engineering Research Council of Canada is gratefully acknowledged.

Note added.—We refer the reader to current theoretical work on the topic by Hui and Jagota [39].

*dalnoki@mcmaster.ca

[1] C. Py, P. Reverdy, L. Doppler, J. Bico, B. Roman, and C. N. Baroud, Phys. Rev. Lett. **98**, 156103 (2007).
[2] N. Patra, B. Wang, and P. Král, Nano Lett. **9**, 3766 (2009).
[3] J. van Honschoten, J. Berenschot, T. Ondarcuhu, R. Sanders, J. Sundaram, M. Elwenspoek, and N. Tas, Appl. Phys. Lett. **97**, 014103 (2010).
[4] J. Bae, T. Ouchi, and R. C. Hayward, ACS Appl. Mater. Interfaces **7**, 14734 (2015).
[5] O. Campàs, T. Mammoto, S. Hasso, R. A. Sperling, D. O'Connell, A. G. Bischof, R. Maas, D. A. Weitz, L. Mahadevan, and D. E. Ingber, Nat. Methods **11**, 183 (2014).
[6] J. B. Grotberg and O. E. Jensen, Annu. Rev. Fluid Mech. **36**, 121 (2004).
[7] A. L. Hazel and M. Heil, Proc. R. Soc. A **461**, 1847 (2005).
[8] C. Duprat, S. Protiere, A. Y. Beebe, and H. A. Stone, Nature (London) **482**, 510 (2012).
[9] J. Bico, B. Roman, L. Moulin, and A. Boudaoud, Nature (London) **432**, 690 (2004).
[10] A. Fargette, S. Neukirch, and A. Antkowiak, Phys. Rev. Lett. **112**, 137802 (2014).
[11] S. Shojaei-Zadeh, S. R. Swanson, and S. L. Anna, Soft Matter **5**, 743 (2009).
[12] R. W. Style, Y. Che, S. J. Park, B. M. Weon, J. H. Je, C. Hyland, G. K. German, M. P. Power, L. A. Wilen, J. S. Wettlaufer *et al.*, Proc. Natl. Acad. Sci. U.S.A. **110**, 12541 (2013).
[13] A. Chakrabarti and M. K. Chaudhury, Langmuir **29**, 6926 (2013).
[14] R. W. Style and E. R. Dufresne, Soft Matter **8**, 7177 (2012).
[15] R. Style, R. Boltyanskiy, Y. Che, J. Wettlaufer, L. A. Wilen, and E. Dufresne, Phys. Rev. Lett. **110**, 066103 (2013).
[16] A. Marchand, S. Das, J. H. Snoeijer, and B. Andreotti, Phys. Rev. Lett. **109**, 236101 (2012).
[17] S. J. Park, B. M. Weon, J. S. Lee, J. Lee, J. Kim, and J. H. Je, Nat. Commun. **5**, 4369 (2014).
[18] T. Young, Phil. Trans. R. Soc. A **95**, 65 (1805).
[19] F. E. Neumann, *Vorlesungen über die Theorie der Capillarität* (BG Teubner, Leipzig, 1894).
[20] P. de Gennes, F. Brochard-Wyart, and D. Quere, *Capillarity and Wetting Phenomena* (Springer, New York, 2008).
[21] G. Lester, J. Colloid Sci. **16**, 315 (1961).
[22] R. Pericet-Cámara, A. Best, H. J. Butt, and E. Bonaccurso, Langmuir **24**, 10565 (2008).
[23] E. R. Jerison, Y. Xu, L. a. Wilen, and E. R. Dufresne, Phys. Rev. Lett. **106**, 186103 (2011).
[24] C.-Y. Hui and A. Jagota, Proc. R. Soc. A **470**, 20140085 (2014).
[25] J. Huang, M. Juszkiewicz, W. H. de Jeu, E. Cerda, T. Emrick, N. Menon, and T. P. Russell, Science **317**, 650 (2007).
[26] N. Nadermann, C.-Y. Hui, and A. Jagota, Proc. Natl. Acad. Sci. U.S.A. **110**, 10541 (2013).
[27] C.-Y. Hui, A. Jagota, N. Nadermann, and X. Xu, Procedia IUTAM **12**, 116 (2015).
[28] See Supplemental Material at http://link.aps.org/supplemental/10.1103/PhysRevLett.115.206101 for a more detailed overview of the sample preparation, a plot of θ_d and θ_b vs T_{in}/γ for PEG atop SIS with the prediction of Eq. (2) included, and a plot supporting the assumption that T is the same in the film under the droplet and outside the droplet.
[29] The tension in the film is a result of the sample preparation and is not found to change appreciably as droplets are deposited.
[30] G. Korosi and E. Kovats, J. Chem. Eng. Data **26**, 323 (1981).
[31] D. R. Lide, *CRC Handbook of Chemistry and Physics* (CRC Press, Boca Raton, 2004), p. 6.
[32] M. J. Colbert, A. N. Raegen, C. Fradin, and K. Dalnoki-Veress, Eur. Phys. J. E **30**, 117 (2009).
[33] A. N. Raegen, K. Dalnoki-Veress, K.-T. Wan, and R. A. L. Jones, Eur. Phys. J. E **19**, 453 (2006).
[34] In these experiments, $T_{\text{in,glyc}}$ was measured on the film either before or after the pipette measurements had been taken, but no systematic difference in T_{pip} with respect to the order of the measurements was found. Both measurements were performed on the same film with the exception of the thinnest SIS and PnBMA films which were too fragile to be subject to both measurements without damaging the integrity of the samples.
[35] A. Chakrabarti and M. K. Chaudhury, Langmuir **31**, 1911 (2015).
[36] B. Zuo, F. F. Zheng, Y. R. Zhao, T. Chen, Z. H. Yan, H. Ni, and X. Wang, Langmuir **28**, 4283 (2012).
[37] S. Wu, J. Phys. Chem. **74**, 632 (1970).
[38] L.-H. Lee, J. Polym. Sci. Pol. Phys. **5**, 1103 (1967).
[39] C.-Y. Hui and A. Jagota, Soft Matter, doi:10.1039/C5SM02157J (2015).

Liquid Droplets on a Highly Deformable Membrane: Supplemental Information

Rafael D. Schulman[1] and Kari Dalnoki-Veress[1, 2, *]

[1] *Department of Physics and Astronomy, McMaster University, 1280 Main St. W, Hamilton, ON, L8S 4M1, Canada*

[2] *Laboratoire de Physico-Chimie Théorique, UMR CNRS Gulliver 7083, ESPCI, Paris, France*

(Dated: October 18, 2015)

SUPPLEMENTARY METHODS

Elastomeric films were prepared from a styrene-isoprene-styrene (SIS) triblock copolymer (Sigma-Aldrich) with a 14% styrene content. Solutions of SIS in toluene (Fisher Scientific, Optima grade) were prepared with various weight fractions. Upon spincoating these solutions, the triblock copolymers self-assemble to form an elastomeric material in which the matrix is composed of polyisoprene while the polystyrene segments form glassy spheres which serve as physical crosslinks. The SIS solutions were spincoated onto freshly cleaved mica substrates (Ted Pella Inc.) to produce uniform (<10% variation) films with thicknesses in the range of $h \sim 280$ nm - 3500 nm, measured using ellipsometry (Accurion, EP3). The films were floated onto the surface of an ultrapure water bath (18.2 MΩ·cm, Pall, Cascada, LS) and subsequently picked up by a circular metal washer to produce free-standing films 3 mm in diameter. Free-standing glassy films of poly(n-butyl) methacrylate (PnBMA) with number averaged molecular weight $M_n =$ 66 kg/mol and polydispersity index PI = 1.05 (Polymer Source Inc.) of thicknesses in the range of $h \sim 65$ nm - 140 nm (with <5% variation) were made following the same protocol. These free-standing films were heated above the glass transition (at 42°) for 1 min to eliminate wrinkles and ensure the films were taut. For the liquid droplets, we use glycerol (Caledon Laboratories Ltd.) and polyethylene glycol (PEG) with $M_n = 0.6$ kg/mol (Sigma-Aldrich).

SUPPLEMENTARY RESULTS

Contact angle experiments on SIS were performed using both glycerol and PEG. In Fig. S1, we plot θ_d and θ_b as a function of T_{in}/γ for both glycerol (red) and PEG (blue) atop SIS. The circle markers indicate droplet contact angles, while bulge contact angles are represented by square markers. Evidently, the contact angle data of PEG assumes the same qualitative behaviour as the glycerol data, but the PEG contact angles are smaller due to the smaller Young's angle atop a supported SIS substrate. In Fig. S1, the theoretical predictions for the contact angles are plotted as solid curves for θ_d and dashed curves for θ_b. We see that the PEG data is also in excellent agreement with the theoretical predictions.

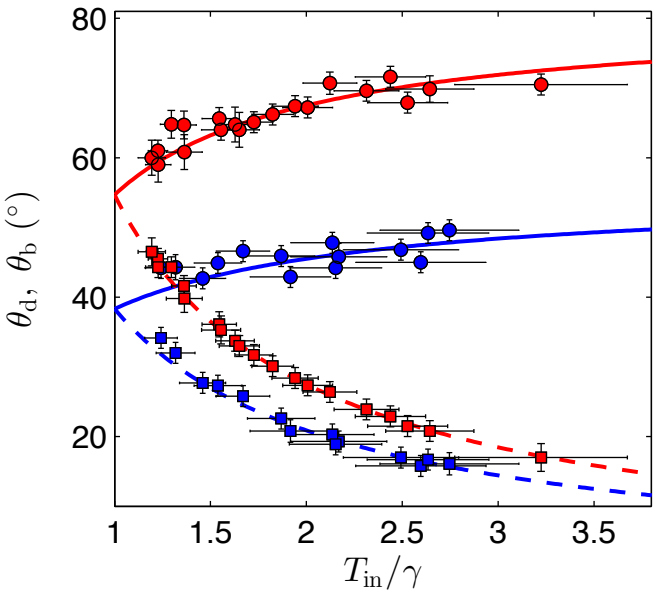

FIG. S1. The droplet and bulge contact angles as a function of the normalized tension atop SIS films. The red markers correspond to glycerol and the blue markers correspond to PEG. Circle markers indicate droplet contact angles and square markers indicate bulge contact angles. The curves represent theoretical predictions from Eq. 2 in the main text for glycerol on SIS (red) and PEG on SIS (blue), where the appropriate θ_y has been inputted. Solid curves indicate predictions for θ_d and dashed curves indicate predictions for θ_b.

In developing our theoretical prediction, we make the reasonable assumption that the mechanical tension in the film is the same in the portion of the film directly below the droplet and in the undeformed film. In fact, we find the theoretical predictions to be very sensitive to this assumption. In Fig. S2, θ_d (circle markers) and θ_b (square markers) are plotted against T_{in}/γ for glycerol atop SIS. The red curves correspond to the theoretical predictions (given by Eq. 2 in the main text) for the droplet (solid curve) and bulge (dashed curve) contact angles. Now, if we enforce that the mechanical tension in the two regions differs by as little as 5 mN/m in our model, we attain new predictions for the contact angles, shown in blue in Fig. S2. Upper/lower blue curves for θ_d and θ_b correspond to the mechanical tension being smaller/larger in the undeformed film compared to the film below the droplet. A 5 mN/m tension change corresponds to only

7% of $T_{\rm in}$ for the lowest tension data on the plot and 2.5% for the highest tension data. We see that even for a small change in the tension, the curves systematically deviate from the data. In addition, this systematic difference grows larger as the tension change is increased. Evidently, even a small difference in T for the two regions causes the theory to fail systematically, indicating that our data is fully consistent with the assumption we have made.

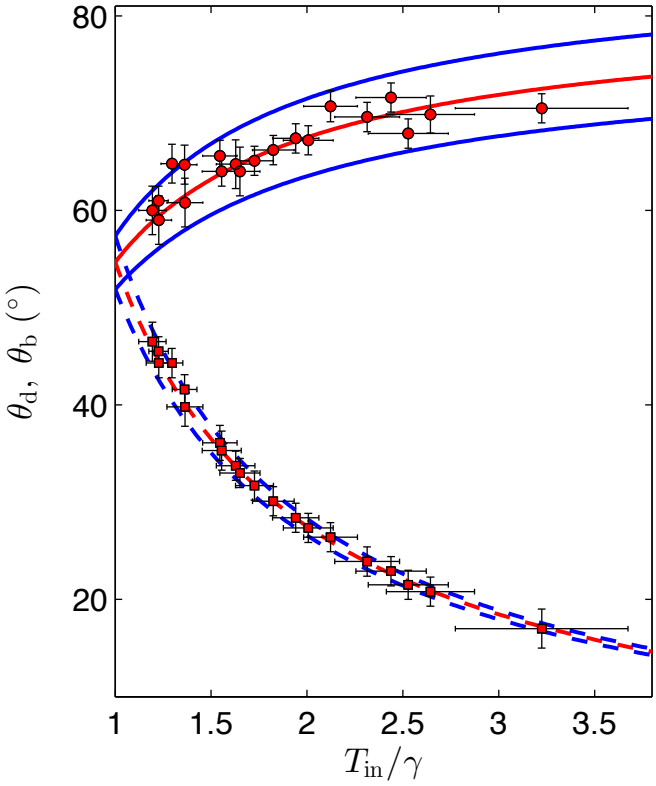

FIG. S2. The droplet and bulge contact angles as a function of the normalized tension for glycerol atop SIS films. Circle markers indicate droplet contact angles and square markers indicate bulge contact angles. The curves represent theoretical predictions from Eq. 2 in the main text for glycerol on SIS, where solid curves indicate predictions for $\theta_{\rm d}$ and dashed curves indicate predictions for $\theta_{\rm b}$. The blue curves represent the theoretical curves when T is enforced to be different by 5 mN/m in the two regions. Upper/lower blue curves for $\theta_{\rm d}$ and $\theta_{\rm b}$ correspond to T being smaller/larger in the region outside the droplet compared to inside.

* dalnoki@mcmaster.ca